Contributed Paper

Electron Cyclotron Emission Diagnostics in the Large Helical Device

NAGAYAMA Yoshio, KAWAHATA Kazuo, INAGAKI Shigeru, KUBO Shin,
NARIHARA Kazumichi, OHYABU Nobuyoshi and the LHD Group
National Institute for Fusion Science, 322-6 Oroshi, Toki 509-5292, Japan

(Received 20 December 2002 / Accepted 17 April 2003)

Abstract

Electron cyclotron emission (ECE) diagnostics have been developed in the Large Helical Device (LHD). The ECE is transmitted from the antenna to the spectrometer for 80 m by means of a corrugated waveguide system, which has a small transmission loss (~30%) in LHD. Although the field angle changes from –40 to +30 degrees on the sight-line of the ECE antenna, it has been observed that the polarization of ECE, which is determined at the plasma edge in LHD, is identical for all frequencies. Thus, the electron temperature profile can be measured using the second harmonic X-mode of ECE. The ECE measured by the Michelson is calibrated with a hot source in order to reduce noise. The ECE temperature measurement agrees well with the Thomson scattering measurement over a wide range of electron densities. The radiometer is cross-calibrated to the Michelson, and is employed for the study of fast phenomena such as internal transport barrier (ITB) formation. Tangentially emitted ECE, in addition to the normal ECE, is investigated in LHD in order to explore the potential of ECE diagnostics.

Keywords:
LHD, ECE, plasma diagnostics, electron temperature, ITB, corrugated waveguide, tangential emission

1. Introduction

The electron cyclotron emission (ECE) measurement is one of the useful diagnostics for the local electron temperature [1-3]. If the ECE is the black body radiation, which is usually a good approximation in high temperature and high density plasmas, the intensity is proportional to the electron temperature and the frequency is proportional to the magnetic field. In tokamaks, ECE diagnostics are employed as a powerful tool to study magnetohydrodynamic (MHD) instabilities because ECE has a capability of continuous measurement with high time resolution [4,5]. Recently, the helical system has been recognized as a strong alternative concept since it has a potential to be a steady state fusion reactor. The world largest helical device is the Large Helical Device (LHD), which has a major radius of R_{ax} = 3.5–3.9 m, an averaged minor radius of a_p = 0.6–0.65 m, and a magnetic field of B_{ax} = 2.6–2.9 T [6]. From the viewpoint of ECE diagnostics, the major differences between the LHD and the tokamak are as follows: (a) the magnetic field profile is peaked in LHD and monotonous in tokamaks for the major radius R; (b) the angle of the magnetic field changes from –40 to +30 degrees in LHD, whereas it is almost constant in tokamaks. The development of ECE diagnostics in LHD, although challenging, has been reported [7-12].

This paper will present an overview of recent progress in ECE diagnostics in LHD. Improvements

author's e-mail: nagayama@nifs.ac.jp

This article is based on the invited talk at the 19th Annual Meeting of JSPF (November 2002, Inuyama).

over the previous system that are shown in those reviews [7,9] are as follows: (1) Two antennas, an inboard side one and a tangential one, have been installed beside the original outboard side antenna; (2) A high frequency heterodyne radiometer has been installed so that fast phenomena can be investigated; (3) The calibration technique has been significantly improved, and consequently the ECE diagnostics and the Thomson scattering are consistent for the electron temperature measurement. In Sec. **2**, the LHD configuration and the ECE measurement system will be presented. The polarization will be investigated. In Sec. **3**, the calibration will be presented. The hot radiation source is used to calibrate the temperature. The ECE measurement and the Thomson scattering measurement for specific electron temperature will be compared. The radiometer is cross-calibrated to the Michelson, and is employed for the study of fast phenomena. In Sec. **5**, the time evolution of the ITB transition will be presented as an example of the application of ECE diagnostics in LHD. In Sec. **6**, the ECE in the tangential direction will be presented as an example of new development of the ECE diagnostics in LHD.

Figure 1(a) shows the contour plots of the strength of magnetic field ($|B|$) and the flux surfaces in the vacuum at the ECE port section in LHD. Figures 1(b) and (c) shows the angle and the $|B|$ of the magnetic field on the viewing line of the ECE diagnostics, respectively. Here, R_{ax} = 3.6 m and B_{ax} = 2.8 T are assumed. The magnetic field profile is peaked in LHD. The angle of the magnetic field changes from –40 to +30 degrees on the viewing line of the ECE diagnostics. Given that the second harmonic ECE has a polarization perpendicular to the magnetic field, the angle of the magnetic field is important in the ECE diagnostics.

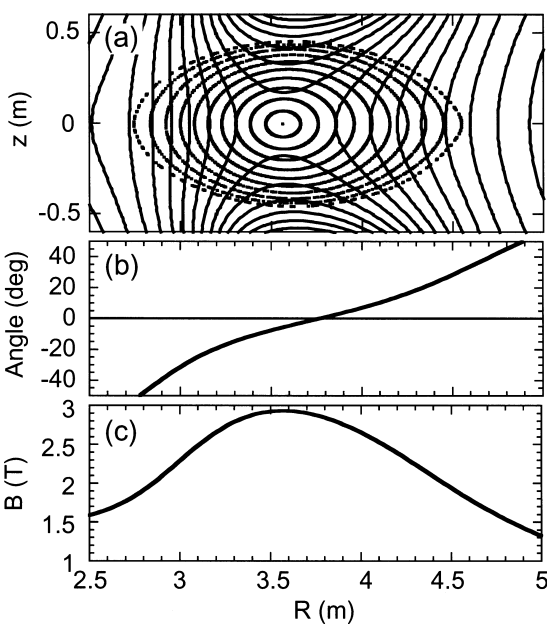

Fig. 1 (a) Contour plot of $|B|$ (solid contours) and flux surfaces (dotted contours) in the plasma cross-section. (b) Angle of the magnetic field. (c) Magnetic field on the viewing line of ECE diagnostics in the case of R_{ax} = 3.6 m and B_{ax} = 2.8 T in LHD.

2. ECE Measurement System

Figure 2 shows a schematic diagram of the ECE measurement system in LHD. In LHD, two antennas are installed, one on the inboard side and one on the outboard side, in order to measure the full profile of the electron temperature. The HE_{11} mode selected has a high transmittance, and the HE_{11} mode at the end of the waveguide couples well to the Gaussian beam in the free space [13,14]. The waist of the Gaussian beam is ~60% of the diameter of the corrugated waveguide. The antenna is designed such that the 100 GHz microwave has a beam waist of 38 mm at the inlet of the waveguide and one of 80 mm at the R = 3.95 m in the plasma. Notch filters for 84 GHz and 82.6 GHz are installed behind a short waveguide at the front end of the corrugated waveguide in order to reduce leakage of the ECH microwave. Each notch filter is an interference filter made of 200 sheets of 25-μm thick polypropylene film. The transmission loss is more than 30 dB, and the full width of the transmission loss of each filter is ~1 GHz. Notch filters in the rectangular waveguide in front of the radiometer attenuate by 40 dB at 82.6 GHz and

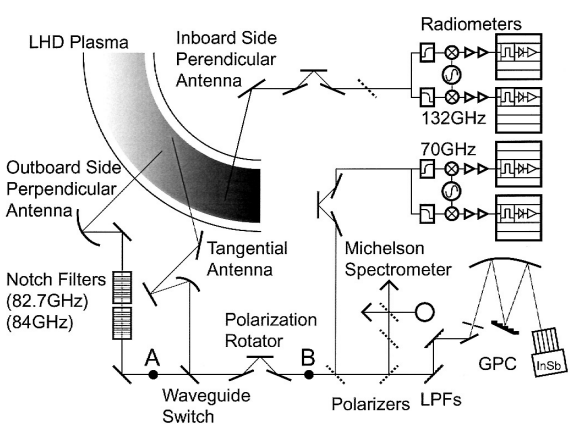

Fig. 2 Schematic diagram of the ECE measurement system in LHD.

84 GHz, with a full width of ~0.5 GHz [7].

The second harmonic X-mode ECE received by the antenna on the outboard side is measured with the fast scanning Michelson interferometer (Michelson) and with the grating polychromator (GPC) [11]. In the Michelson, a rooftop mirror in the interferometer oscillates with an active scan length of 4.6 cm and with a scanning frequency of 20 Hz. Each scan produces an interferogram, which is to be Fourier-transformed to produce the spectrum of the ECE signal from ~60 GHz to 300 GHz [7]. The LC filter for the driving motor of the Michelson, which was reported in Ref. [7], has been taken out. The electromagnetic interference (EMI) is significantly reduced by filling the space between the cryostat of the InSb detector and the preamplifier case with an aluminum ring.

The fundamental O-mode ECE received by the outboard antenna is separated by a wiregrid beam splitter and is measured with the low frequency radiometer. The second harmonic X-mode ECE received by the inboard antenna is measured with the high frequency radiometer. Figure 3 shows the schematic diagram of the heterodyne radiometer system used in LHD [12]. The high frequency radiometer and the low frequency one have the same structure except the notch filter and the frequency of the local oscillator. The notch filter is not installed in the high frequency radiometer but in the low frequency radiometer [7]. The high frequency radiometer has a local oscillator at 132 GHz and covers a frequency range between 106 and 158 GHz, whereas the low frequency radiometer has a local oscillator at 70 GHz and covers a frequency range between 53 and 87 GHz. Data of the GPC and radiometers are taken with both slow and fast CAMAC digitizers with 12 bits ADC. The sampling rates of the slow and fast digitizers are 10 kHz and 200 kHz, respectively. The high frequency noise in the slowly sampled signal is reduced by an RC low pass filter with a time constant of τ = 33 μs.

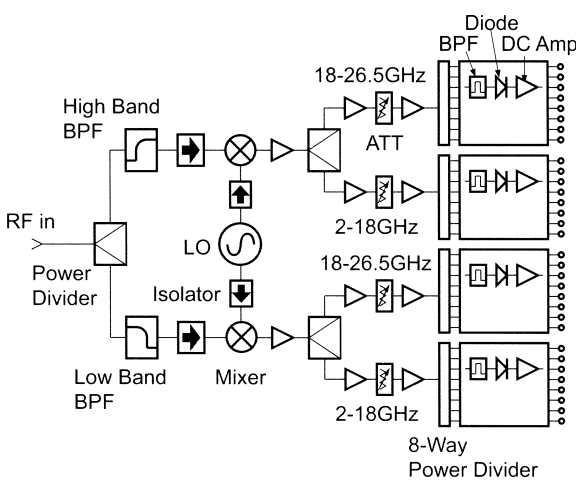

Fig. 3 Schematic diagram of the heterodyne radiometer system in LHD. BPF indicates the band pass filter. LO indicates the local oscillator. ATT indicates the variable attenuator.

The ECE is transferred from the antenna in the LHD hall to the spectrometers in the diagnostics room. The length of the transmission line is ~80 m. In order to reduce transmission loss, a corrugated waveguide system [13,14] is utilized in the ECE measurement system in LHD. The waveguide has an inner wall with a diameter of 63.5 mm and rectangular grooves with a depth of 0.43 mm, width of 0.46 mm, and period of 0.66 mm. It is designed to transfer a microwave with a frequency between 50 and 220 GHz. Figure 4(a) shows the spectra of the hot radiation source in the LHD hall (point A in Fig. 2) and in the diagnostic room (point B in Fig. 2). Figure 4(b) shows the transmittance of the corrugated waveguide system, which is the ratio of these spectra. By use of the corrugated waveguide system, transmission loss is ~30% from the LHD hall to the diagnostics room.

As is described in Sec. **1**, the angle θ of the magnetic field varies from –40 to +30 degrees in LHD. The ECE propagation is calculated numerically, with the assumption that the electron temperature profile is parabolic and the electron density profile is flat. The theoretical result is as follows: if the electron density sharply drops to zero at the plasma edge, the ECE polarization is determined at the plasma edge. Usually, these are good assumptions in LHD. A universal polarization rotator is set in each waveguide system, and

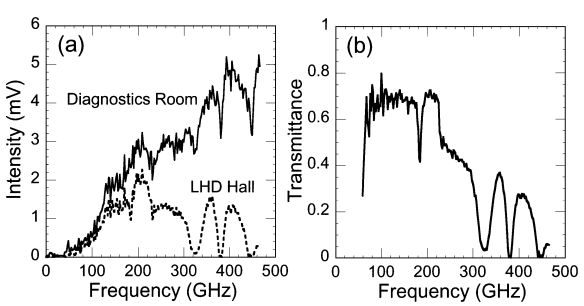

Fig. 4 The transmittance of the corrugated waveguide system that is installed from the LHD hall to the diagnostic room.

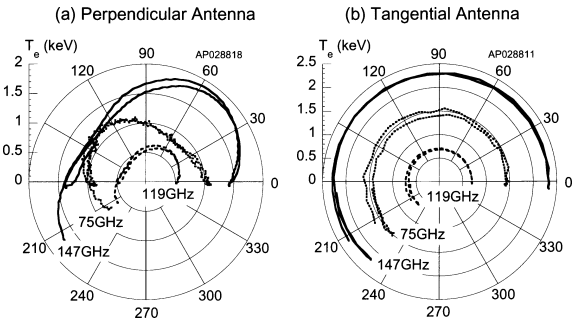

Fig. 5 (a) Polarization of the ECE received by the perpendicular antenna. (b) Polarization of the ECE received by the tangential antenna.

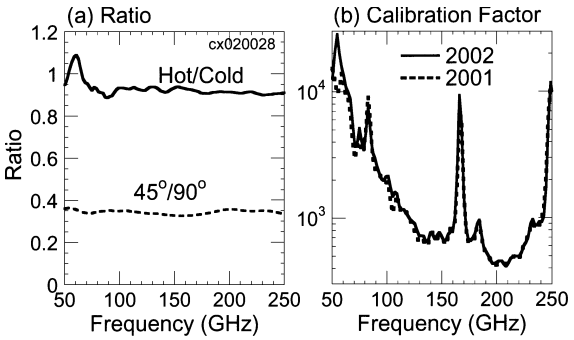

Fig. 6 (a) The ratio of the emissivity of the hot radiation source to the cold source (Hot/Cold), and the ratio of the transparence of the 45-degree polarizer to the 90-degree polarizer (45°/90°). (b) Calibration coefficients in FY2001 and FY2002.

consists of a standard 90-degree miter bend between two 135-degree miter bends. This device rotates the polarization of linearly polarized incident radiation by two times the angle between the plane of these miter bends and the incident electric field. During long-pulse operation, the universal polarization rotator is turned by a pulse motor. Figure 5(a) shows the polarization of the ECE of different frequencies received by the perpendicular antenna. Although the field angle changes spatially, the second harmonic ECE in the wide frequency range has constant polarization, as expected based on the above discussion. The fundamental ECE also has a single polarization, which is 90 degrees different from the second harmonics. Therefore, the fundamental ECE is mainly O-mode, the second harmonics mainly X-mode. Figure 5(b) shows that the ECE received by the tangential antenna is not linearly polarized.

3. Calibration

The ECE antenna consists of a concave mirror and a convex mirror. When calibration is performed, the concave mirror rotates 180 degrees to reflect a hot (873 K) radiation source. For purposes of calibration, a polarizer that is set at 45 degrees in the plasma experiment is set at 90 degrees to increase the calibration signal, and to reduce the bit-noise, an active low-pass filter is additionally used. The active low-pass filter has a gain of 200 and it cuts any frequency higher than 100 kHz. The scanning frequency of Michelson is 5 Hz in the case of calibration, since it works almost continuously. The one million scans of the interferogram signal of the Michelson are integrated for the calibration. The interferogram of the room temperature radiation is subtracted from that of the hot/cold source. The Fourier transform of the subtracted interferogram gives the frequency spectrum of the hot/cold radiation.

Figure 6(a) shows the ratio of the emissivity of the hot radiation source to the cold (77 K) source. The hot source is a plane ceramic heater with an area of 25-cm square. The cold source is a liquid nitrogen-cooled foam absorber. The *Hot*/*Cold* ratio is defined as

$$Hot/Cold = \frac{I_{\mathrm{hot}}}{I_{\mathrm{cold}}} \frac{(T_{\mathrm{room}} - T_{\mathrm{cold}})}{(T_{\mathrm{hot}} - T_{\mathrm{room}})}, \qquad (1)$$

where I_{hot} and I_{cold} are the spectrum of the hot and cold sources, respectively, from which the room temperature radiation is subtracted, and T_{room}, T_{cold} and T_{hot} are the temperature of the room, that of the cold source, and that of the hot source, respectively. The emissivity of the hot source is ~90%. Figure 6(a) also shows the ratio of the transmittance of the 45-degree polarizer to the 90-degree polarizer. The calibration coefficient *Calb* is determined from these factors, the spectrum of the radiation of the hot source I_{antenna}, from which the radiation of the room temperature is subtracted, and the gain of the active filter *Amp*, as

$$Calb = \frac{(T_{\mathrm{hot}} - T_{\mathrm{room}})}{I_{\mathrm{antenna}}} \cdot Amp \cdot \frac{Hot/Cold}{45°/90°}. \qquad (2)$$

Figure 6(b) shows frequency distributions of the calibration coefficient measured in the years 2001 and 2002. The annual change of the calibration factor looks very small in LHD.

4. Electron Temperature

Figure 7 shows the electron temperature profile measured using ECE and Thomson scattering in the cases of lower β and higher β, respectively. The radio-

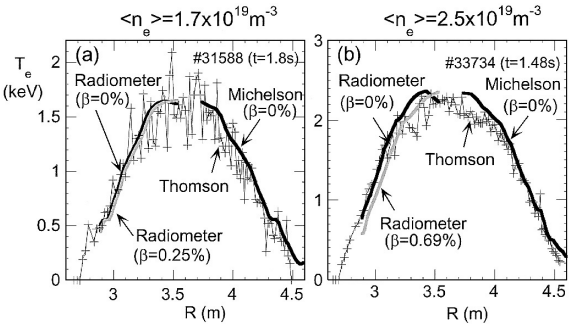

Fig. 7 (a) The electron temperature profile measured by the Thomson scattering (+) and the ECE diagnostics in the case of lower beta. (b) The electron temperature profile measured by the Thomson scattering and the ECE in the case of higher beta.

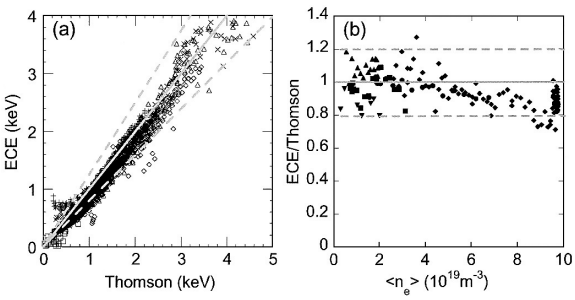

Fig. 8 (a) Comparison of the electron temperature measured with the Thomson scattering and the ECE diagnostics. (b) The ratio of the ECE and the Thomson scattering for the various lineaveraged electron densities. The gray line indicates $T_{ECE} = T_{Thomson}$. The broken lines indicate a discrepancy of ±20%.

meter data are cross-calibrated to the Michelson under the assumption that the electron temperatures are identical at the same ρ. Here, ρ is the normalized minor radius. The ρ is obtained using the equilibrium code, VMEC [15]. It is derived that the magnetic axis should be shifted to the outboard side when the β is not negligible. However, the electron temperature profile measured with the Thomson or the Michelson is not shifted to the outboard side. Considering the radial shift caused by the β effect when cross-calibrating, the electron temperature profile obtained with the radiometer is shifted to the outboard side relative to the temperature profile measured by the Thomson scattering, as shown in Fig. 7(a). Since the radial discrepancy reduces as the β decreases, as shown in Fig. 7(b), this discrepancy is not due to measurement error of the position. Therefore, the $\beta = 0$ is assumed when cross-calibrating the radiometer data to the Michelson in LHD.

Figure 8(a) plots the electron temperature measured by ECE versus that measured by the Thomson scattering when B_{ax} = 2.8 T and R_{ax} = 3.6 m. In Fig. 8(a), the electron temperatures at different radii are plotted. In Fig. 8(b), the ratio of the electron temperature at $\rho = 0.2$ measured by the ECE to that by the Thomson scattering is plotted versus the line-averaged electron density. The electron temperatures measured by the ECE and the Thomson, respectively, agree within ±20% for a wide range of density. In the case of very low density ($n_e < 0.6 \times 10^{19}$ m^{-3}), the ECE temperature is higher than the Thomson temperature due to the synchrotron emission from the fast electrons. In the case of high density, the ECE temperature looks slightly lower than the Thomson temperature. It has been observed that ECE temperature starts to decrease as the density increases when $n_e > 0.6\ n_c$ in LHD, where n_c is the cut-off density of the X-mode [10]. The density limit of the ECE measurement in LHD is less than that in tokamaks, because the ECE ray is diffused due to the twisted plasma structure in LHD. In this case, the ECE diagnostics should be affected when $n_e > 1 \times 10^{20}$ m^{-3}. Therefore, the ECE measurement may not be affected in the density range shown in Fig. 8(b).

5. Study of ITB Using ECE Diagnostics

Using the radiometer data cross-calibrated to the Michelson, the time evolution of the electron temperature profile can be obtained. Figure 9(b) shows the time evolution of the electron temperature profile obtained with the high frequency radiometer when the ITB is generated. In this case, the radiometer data is cross-calibrated to the Michelson data at t = 2.8 sec assuming $\beta = 0$. In this shot, the counter-NBI is injected between t = 0.5 and 2.3 sec, the ECH is injected from 2 to 2.6 sec, and the plasma is initiated at t = 2 sec. The ECE intensity corresponding to $\rho > 0.6$ is enhanced due to non-thermal emission, which results when the electron density is so low ($\langle n_e \rangle \sim 0.5 \times 10^{19}$ m^{-3}). Figure 9(c) shows the electron temperature profiles when a small ITB is established (t = 2.4 sec) and, in contrast, when a large ITB is established (t = 2.6 sec). The radii of the small ITB and the large ITB are $R \sim 14$ cm ($\rho \sim 0.23$) and $R \sim 25$ cm ($\rho \sim 0.43$), respectively. In the case of counter-NBI heating, the electron temperature profile in the core region is usually flat, and the small ITB can

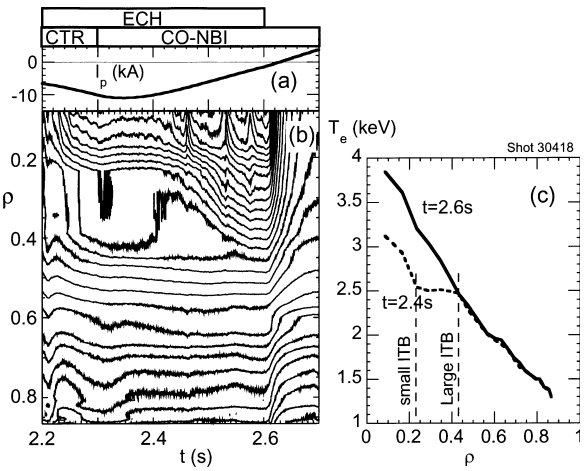

Fig. 9 (a) Time evolution of the plasma current when the ITB is generated. (b) Contour plot of the time evolution of the electron temperature profile measured by the ECE diagnostics. The contour step is 0.1 keV.

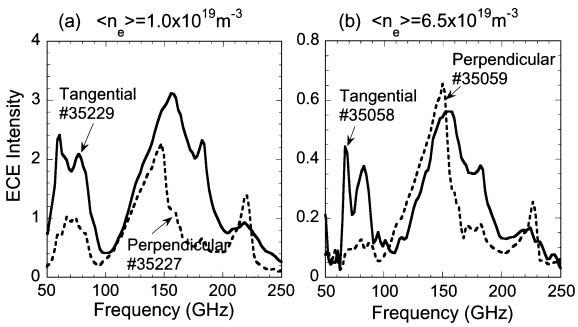

Fig. 10 (a) Comparison of the spectrum of ECE received by the tangential antenna and by the perpendicular antenna in the case of low density plasma. (b) Comparison of the spectrum of ECE received by the tangential antenna and that by the perpendicular antenna in the case of high density plasma.

be generated by the ECH. In the case of co-NBI heating, a large ITB can be generated by the ECH.

The ITB region starts to expand ~100 msec after switching from the counter-NBI to the co-NBI, and it takes another ~100 msec for the large ITB to be established. The time evolution of the plasma current is shown in Fig. 9(a). Because the plasma current is still negative when the ITB radius increases, the ITB size expands due to the direction of NBI. Based on the fact that the electron temperature does not change in the outside of the large ITB, a different transport mechanism may govern the regions inside and those outside the large ITB. The upper limit of the ITB radius is determined by an unknown mechanism. The results of this experiment indicate that the ECE diagnostics has great potential for the study of ITB physics in LHD.

6. Tangential ECE

Due to the peaked $|B|$ profile, the electron temperature at the plasma center cannot be measured using the perpendicular antenna. The $|B|$ profile is monotonic on the sight-line from the port, where the $|B|$ is minimum, to the helical coil, where the $|B|$ is maximum. Therefore, using the tangential antenna, it might be possible to measure the central electron temperature. The tangential antenna is newly installed in LHD. By use of a waveguide switch, the tangential antenna is connected to the waveguide system for the outboard antenna. The ECE received by the tangential antenna is measured by the Michelson. Figure 10 shows the spectrum of the ECE received by the tangential antenna and the perpendicular antenna. In the case of low density, the spectrum of the tangentially received ECE is symmetric, and the peak frequency is higher than that of the normal ECE. This indicates that, as expected, the tangential antenna receives the ECE from a higher $|B|$ than that in the port section. The tangential ECE is not polarized, as shown in Fig. 5(b). Thus, the spectrum of the tangential ECE shown in Fig. 10 includes both the O-mode and the X-mode, whereas the X-mode is selected for the normal ECE shown in Fig. 10. In the case of high density, the intensity of the tangential ECE is lower than that of the normal ECE. The reason for this may be that the ECE ray is diffused due to the twisted plasma structure in LHD. Interestingly, the intensity of the tangential ECE in the fundamental frequency region (≤ 100 GHz) is comparable to that of the second harmonics, whereas the normal ECE less than 100 GHz is almost disappeared due to the cut-off.

7. Summary

In summary, an ECE measurement system based on the corrugated waveguide system has been developed in LHD. Transmission loss was observed to be ~30% for the ECE transmission line with a length of ~80 m. Because the polarization of ECE is determined at the plasma edge in LHD, the electron temperature profile can be obtained from the second harmonic X-mode of ECE. The electron temperature profile is calibrated with a hot source in order to reduce noise. The emissivity of the hot source is ~90%, and this is taken into account to

obtain the calibration coefficient. The electron temperature profile obtained by the ECE diagnostics agrees well with the Thomson scattering measurement over a wide range of electron density. The radiometer is cross-calibrated to the Michelson, and is employed for the study of fast phenomena such as the ITB formation process. It has been observed that the ITB radius expands after switching from the counter-NBI to the co-NBI. Tangentially emitted ECE diagnostics are being developed in LHD in order to explore the potential of ECE diagnostics. Further study is required to interpolate the spectrum of the tangentially emitted ECE.

Acknowledgments

The authors are grateful to Dr. H. Sasao, Dr. P.C. de Vries, Mr. Y. Ito, Mr. M. Koike, Mr. S. Sugito, and Mr. K. Yamauchi for their technical support. The authors are also grateful to Prof. A. Mase, Prof. H. Hojo, Prof. T. Maekawa and Prof. K. Nagasaki for useful discussion. The authors would like to thank Prof. S. Sudo and Prof. O. Motojima for their continuous encouragement. This work was partially supported by Grant-in-Aid for Scientific Research (B), (No.11480116, 1998) from the Ministry of Education, Science, Sports and Culture of Japan.

References

[1] A.E. Costley, R.J. Hastie, J.W.M. Paul and J. Chamberlain, Phys. Rev. Lett. **33**, 758 (1974).

[2] M. Bornatici, R. Cano, O. De Barbieri and F. Engelmann, Nucl. Fusion **23**, 1153 (1983).

[3] I.H. Hutchinson, *Principles of Plasma Diagnostics*, (Cambridge Univ. Press, 1987).

[4] Y. Nagayama, M. Yamada, W. Park, E.D. Fredrickson, A.C. Janos, K.M. McGuire and G. Taylor, Phys. Plasmas **3**, 1647 (1996).

[5] Y. Nagayama, G. Taylor, E.D. Fredrickson, R.V. Budny, A.C. Janos, D.K. Mansfield, K.M. McGuire and M. Yamada, Phys. Plasmas **3**, 2631 (1996).

[6] M. Fujiwara, K. Kawahata, N. Ohyabu, O. Kaneko, A. Komori *et al.*, Nucl. Fusion **41**, 1355 (2001).

[7] Y. Nagayama, K. Kawahata, A. England, Y. Ito, S. Sugito, N. Bretz, M. McCarthy, G. Taylor, J. Doane, H. Ikeji, T. Edlington and J. Tomas, Rev. Sci. Instrum. **70**, 1021 (1999).

[8] P.C. de Vries, K. Kawahata, Y. Nagayama, H. Sasao, S. Inagaki and K. Nagasaki, Phys. Plasmas **7**, 3707 (2000).

[9] Y. Nagayama, S. Inagaki, H. Sasao, P. de Vries, Y. Ito, K. Kawahata, K. Narihara, I. Yamada and LHD Group, Fusion Eng. Des. **53**, 201 (2001).

[10] H. Sasao, S. Inagaki, Y. Nagayama, P.C. de Vries, K. Kawahata, K.Y. Watanabe, T. Tokuzawa, K. Tanaka, S. Kubo, K. Narihara, A. Komori, H. Yamada, O. Kaneko and O. Motojima, Fusion Eng. Des. **53**, 153 (2001).

[11] K. Kawahata, P.C. de Vries, Y. Nagayama, S. Inagaki, T. Tokuzawa, K. Tanaka and S. Sasao, Rev. Sci. Instrum. **72**, 387 (2001).

[12] K. Kawahata, Y. Nagayama, S. Inagaki, Y. Ito and LHD Experimental Group, *to be published in* Rev. Sci. Instrum. (2003).

[13] J.L. Doane, Infrared Millimeter Waves **13,** 123 (1985).

[14] J.L. Doane and C.P. Moeller, Int. J. Electren. **77,** 489 (1994).

[15] S.P. Hirshman and D.K. Lee, Comput. Phys. Comm. **39,** 143 (1986).